ASHA American Speech-Language-Hearing Association

JSLHR

Research Article

# Collision Pressure and Dissipated Power Dose in a Self-Oscillating Silicone Vocal Fold Model With a Posterior Glottal Opening

**Mohsen Motie-Shirazi,[a] Matías Zañartu,[b] Sean D. Peterson,[c] Daryush D. Mehta,[d] Robert E. Hillman,[d] and Byron D. Erath[a]**

[a]Department of Mechanical and Aeronautical Engineering, Clarkson University, Potsdam, NY [b]Department of Electronic Engineering, Universidad Técnica Federico Santa María, Valparaíso, Chile [c]Department of Mechanical and Mechatronics Engineering, University of Waterloo, Ontario, Canada [d]Center for Laryngeal Surgery and Voice Rehabilitation, Massachusetts General Hospital, Boston

ARTICLE INFO

Article History:
Received September 2, 2021
Revision received January 24, 2022
Accepted May 4, 2022

Editor-in-Chief: Bharath Chandrasekaran
Editor: Jack J. Jiang

https://doi.org/10.1044/2022_JSLHR-21-00471

ABSTRACT

**Purpose:** The goal of this study was to experimentally evaluate how compensating for the adverse acoustic effects of a posterior glottal opening (PGO) by increasing subglottal pressure and changing supraglottal compression, as have been associated with vocal hyperfunction, influences the risk of vocal fold (VF) trauma.
**Method:** A self-oscillating synthetic silicone model of the VFs with an airflow bypass that modeled a PGO was investigated in a hemilaryngeal flow facility. The influence of compensatory mechanisms on collision pressure and dissipated collision power was investigated for different PGO areas and supraglottal compression. Compensatory behaviors were mimicked by increasing the subglottal pressure to achieve a target sound pressure level (SPL).
**Results:** Increasing the subglottal pressure to compensate for decreased SPL due to a PGO produced higher values for both collision pressure and dissipated collision power. Whereas a 10-mm$^2$ PGO area produced a 12% increase in the peak collision pressure, the dissipated collision power increased by 122%, mainly due to an increase in the magnitude of the collision velocity. This suggests that the value of peak collision pressure may not fully capture the mechanisms by which phonotrauma occurs. It was also found that an optimal value of supraglottal compression exists that maximizes the radiated SPL, indicating the potential utility of supraglottal compression as a compensatory mechanism.
**Conclusions:** Larger PGO areas are expected to increase the risk of phonotrauma due to the concomitant increase in dissipated collision power associated with maintaining SPL. Furthermore, the risk of VF damage may not be fully characterized by only the peak collision pressure.

Correspondence to Byron D. Erath: berath@clarkson.edu. ***Disclosure:*** *Dr. Robert E. Hillman and Dr. Daryush Mehta have a financial interest in InnoVoyce LLC, a company focused on developing and commercializing technologies for the prevention, diagnosis, and treatment of voice-related disorders. Dr. Hillman's and Dr. Mehta's interests were reviewed and are managed by Massachusetts General Hospital and Mass General Brigham in accordance with their conflict-of-interest policies. Dr. Matías Zañartu has financial interest in Lanek SPA, a company focused on developing and commercializing biomedical devices and technologies. Dr. Zañartu's interests were reviewed and are managed by the Universidad Técnica Federico Santa María in accordance with its conflict-of-interest policies. All the other authors have declared that no other competing financial or nonfinancial interests existed at the time of publication.*

Incomplete closure of the vocal folds (VFs) has been commonly observed in normal phonation, especially in women (Cielo et al., 2019; Linville, 1992; Patel et al., 2012; Schneider & Bigenzahn, 2003). Incomplete or impaired closure can also be caused by some pathological conditions such as VF paralysis, VF lesions (e.g., nodules and polyps), and muscle tension dysphonia (Choi et al., 2012; Morrison et al., 1983; Nguyen et al., 2009). Incomplete closure of the posterior (nonvibratory) cartilaginous portion of the VFs, which may extend into the (vibratory) membranous portion (Morrison et al., 1986), is described as a posterior glottal opening (PGO).

The presence of a PGO results in persistent airflow leakage during phonation (Holmberg et al., 1988), which changes both the dynamics of VF oscillation and the acoustic output (Birk et al., 2017; G. Chen et al., 2011). Clinical (Holmberg et al., 1988; Perkell et al., 1994) and numerical (Cranen & Schroeter, 1995; Scherer et al., 2013) investigations have demonstrated that the presence of a PGO is highly correlated with an increase in the amplitude of mean flow rate and maximum flow declination rate at the glottis. Acoustically, as the PGO area increases, the voice becomes breathier (Fritzen et al., 1986) with a lower sound pressure level (SPL) (Schneider & Bigenzahn, 2003). Different physiological mechanisms can be implemented to compensate for the undesirable effects of a PGO (e.g., reduced loudness). These include increasing the adduction level of the VFs (Döllinger et al., 2016), raising the subglottal pressure (Åkerlund & Gramming, 1994; Björklund & Sundberg, 2016; Herbst et al., 2015; Isshiki, 1964; Ladefoged & McKinney, 1963), and changing the acoustic loading of the vocal tract by constricting the epilarynx (Titze et al., 2008). Prior work (Galindo et al., 2017) has suggested that raising the subglottal pressure is the most effective compensatory mechanism, which is consistent with numerical and clinical studies showing that for nodules and polyps, which similarly impede complete glottal closure, subglottal pressure is increased (Espinoza et al., 2017, 2020; Morrison et al., 1986). Therefore, increased subglottal pressure is similarly expected to be implemented in individuals with a PGO.

The aforementioned compensatory actions are also correlated with a change in the collision behavior of the VFs and the resultant collision stresses imparted to the VF tissue, also known as contact/collision/impact pressures (Hess et al., 1998; Jiang & Titze, 1994; Mehta et al., 2019). Note that references to both contact and collision pressure can be found in the literature when referring to the pressures that arise during the closing phases of the phonatory cycle. It is proposed that collision pressure is a more appropriate term because it captures the dynamic nature of the process. In contrast, contact pressures may arise due to other scenarios such as static posturing/adduction of the VFs.

Compensatory behaviors also influence the energy dissipated during VF collision, which is characterized by the collision pressure and velocity along the surface of the VF tissue (Motie-Shirazi et al., 2021a; Titze & Hunter, 2015). Abnormally high peak collision pressure has been commonly postulated to play a primary role in the emergence of benign VF lesions (Hillman et al., 1989, 2020). This hypothesis has been supported by showing that high-intensity phonation leads to disruption of the basement membrane of the VFs (Gray & Titze, 1988; Kojima et al., 2014; Levendoski et al., 2014; Rousseau et al., 2011; Zhao et al., 1991). However, it has been argued that high values of dissipated collision power are responsible for increased internal heat and breaking of the molecular bonds of VF tissues (Titze & Hunter, 2015; Titze et al., 2003). As such, dissipated collision power may provide a better indicator of phonotrauma than peak collision pressure. It is not well known how these two measures of damage are influenced by changes in the collision behavior of the VFs in the presence of voice disorders. Consequently, understanding the influence of compensatory behaviors on the VF collision mechanics could shed light on the pathophysiology of collision-related VF pathologies. Specifically, insight into how the peak collision pressure and dissipated collision power vary due to the presence of a PGO could provide insight into the prevention, diagnosis, and treatment of these hyperfunctional voice disorders.

There is limited understanding of how a PGO might contribute to hyperfunctional vocal response and affect VF collision forces. Investigating the effects of incomplete VF closure on VF collision pressure and the associated compensatory mechanisms is prohibitively difficult in vivo. Although technically feasible (Mehta et al., 2021), direct in vivo measurements of VF collision pressure continues to be a challenge due to the physical intrusion of any measurement sensor and the difficulty in achieving stable, repeatable sensor positioning (Gunter et al., 2005; Hess et al., 1998; Verdolini et al., 1999). Simultaneously acquiring the medial VF surface dynamics and dissipated collision power with sufficiently high spatial resolution further complicates the situation. Therefore, alternative approaches, such as numerical and benchtop models, have been employed to overcome the challenges associated with in vivo investigations.

The effect of increasing subglottal pressure as compensation for the adverse consequences of a PGO has been investigated numerically in the context of modeling the vicious cycle of phonotraumatic vocal hyperfunction (Hillman et al., 2020). A posterior airflow bypass was implemented into a lumped-element modeling approach (Zañartu et al., 2014) based on a body cover formulation (Story & Titze, 1995). Increasing the PGO area significantly attenuated the radiated sound SPL. Increasing the subglottal pressure to compensate for the reduced SPL increased the steady and unsteady components of the flow rate to values that were much higher than normal physiological ranges and produced much greater VF collision forces. A subsequent study modeled the effect of both a posterior and membranous opening using an improved triangular body cover lumped-element model while also including the effects of intrinsic laryngeal muscle activation (Galindo et al., 2017). The posterior glottal distance, which denoted the arytenoid displacement, was adjusted to model different sizes of glottal openings. At a fixed subglottal pressure, the SPL initially increased for very small posterior glottal distances and then decreased as the glottal area continued to increase. Compensating for the reduced SPL

resulted in drastic increases (up to 100%) in the flow rate and collision pressure as a function of the posterior glottal distance.

In contrast to prior lumped-element investigations (Galindo et al., 2017; Zañartu et al., 2014), results from a three-dimensional computational model that simulated the effects of incomplete closure (Zhang, 2016) found that increasing the initial angle of the VFs (i.e., introducing a membranous gap) only slightly reduced the SPL. The SPL was found to mainly be dependent on the subglottal pressure. Therefore, a significant increase in the subglottal pressure was not required to compensate for the modest SPL reduction. However, no supraglottal acoustic tract was utilized in these investigations, which may influence the accuracy of the acquired results due to the absence of acoustic loading effects.

Narrowing the epilaryngeal area via supraglottal compression has also been considered as a reactive and/or compensatory behavior during voice production (Galindo et al., 2017; Yanagisawa et al., 1989; Zhang, 2021). Although supraglottal compression is sometimes observed in individuals with normal voices (Behrman et al., 2003; Stager et al., 2000), its acoustic role has been controversial. Numerical analysis has shown that constricting the epilarynx increases the vocal tract impedance to a level comparable to that of the glottis, resulting in a decrease in the oscillation threshold pressure and an increase in the acoustic power (Titze, 2006; Titze et al., 2008; Titze & Story, 1997). A slight increase in the SPL has also been observed to occur by increasing medial compression of the false VFs (Alipour et al., 2007). Recently, studies utilizing a three-dimensional computational model that simulated a simplified source–tract interaction in the epilaryngeal region showed that decreasing the epilaryngeal area resulted in a drastic increase in the SPL when the initial glottal angle was small (Zhang, 2021). That is, a narrower epilarynx resulted in a lower subglottal pressure necessary to produce a target SPL, which resulted in lower values of peak collision pressure. On the other hand, studies of excised human VFs in a hemilaryngeal configuration with a fabricated glass vocal tract found that reducing the epilaryngeal area did not have a significant effect on the SPL (Döllinger et al., 2012) and, in some cases, even decreased the SPL (Döllinger et al., 2006). Finally, lumped-element VF model investigations reported that supraglottal compression did not play a significant role in compensatory outcomes when compared with the effects of subglottal pressure and intrinsic laryngeal muscle activation (Galindo et al., 2017). A minor increase in SPL was found at an optimal value of the epilarynx area, whereas the SPL decreased for suboptimal constriction values that were either too large or small (Galindo et al., 2017).

Unfortunately, a problem that plagues both lumped-element and computational VF models is that, traditionally, the VF collision forces are not solved directly. Instead, they are traditionally prescribed a priori, often relying on simplifying assumptions. In these cases, the accuracy of the VF collision forces is limited by the fidelity of the collision model that is implemented. Initial efforts have sought to assess the accuracy of the collision pressure formulations using a lumped-element model and a Hertzian contact framework (Díaz-Cádiz et al., 2019). However, to the authors' knowledge, rigorous validation of these collision models is lacking, and there is a need to explore advancements, such as incorporating viscoelastic formulations of VF contact (Erath et al., 2017).

Synthetic silicone models of the VFs have been developed as reliable surrogates for investigating aerodynamic, acoustic, and collision behaviors of the VFs. Driven synthetic models have been employed for studying the effect of a PGO on the glottal flow field (Park & Mongeau, 2008), although the influence on VF collision was not explicitly investigated. Self-oscillating synthetic models have been used for wide-ranging applications, such as estimating the energy transfer to the VFs (Motie-Shirazi et al., 2021b; Thomson et al., 2005), investigating acoustic interactions (Migimatsu & Tokuda, 2019; Zhang et al., 2006), studying asymmetric VF behaviors (Zhang et al., 2013; Zhang & Hieu Luu, 2012), and measuring collision pressures (L. Chen & Mongeau, 2011; Horáček et al., 2016; Motie-Shirazi et al., 2019, 2021a; Spencer et al., 2008; Weiss et al., 2013). The advantage of synthetic models is that they do not require a priori prescription of the collision mechanics. Recently, a novel technique was introduced for acquiring high spatial and temporal resolution of the collision pressure in a self-oscillating synthetic silicone VF model (Motie-Shirazi et al., 2019). A method for calculating the dissipated power dose based on the VF kinematics and collision pressure was simultaneously developed (Motie-Shirazi et al., 2021a). This procedure is advantageous in that it can also be implemented to evaluate how the collision power and dissipated power dose are influenced by a PGO when common compensatory behaviors are performed.

This study aims to gain insight into the pathophysiology of phonotraumatic VF damage by quantifying how compensating for a PGO affects VF collision pressure and the power dissipated during collision. Self-oscillating synthetic VF models are used to evaluate the influence of a PGO on glottal aerodynamics, oscillation kinematics, and collision dynamics in a previously validated hemilaryngeal facility (Motie-Shirazi et al., 2019, 2021a, 2021b). The effect of compensating for SPL by raising the subglottal pressure and constricting the epilaryngeal area is investigated, with an emphasis on how these behaviors influence VF collision mechanics. The Method section introduces the experimental setup, describes the measurement procedure, and briefly reviews the process for computing the dissipated power. The results are presented and compared with prior findings in the Results section, and the

implications are discussed in the Discussion section. Finally, the Conclusions section highlights the important findings of this study.

## Method

### Flow Facility

The hemilaryngeal flow facility and the synthetic VF model used in this work were similar to that reported in prior research efforts (Motie-Shirazi et al., 2019, 2021a, 2021b). Figure 1a shows a schematic of the flow facility. Briefly, compressed air at 1,000 kPa was regulated to 17 kPa before passing through a Dwyer RMC 103-SSV inline flow meter that adjusted and measured the mean flow rate. The airflow then entered a cylindrical plenum chamber with a cross-sectional area of 0.06 $m^2$ and a volume of 0.03 $m^3$. The inner walls of the chamber were covered with 20-mm-thick foam to acoustically insulate the chamber. The flow exited the plenum chamber through a 150.0-mm-long tracheal channel with a rectangular cross-sectional area of 213.0 $mm^2$. A Kulite ET-3 DC pressure transducer was flush-mounted in the wall 30.0 mm upstream of the exit of the tracheal channel and recorded the time-varying static subglottal pressure.

A mounting bracket was bolted to the exit of the tracheal channel. A silicone VF model was secured in the bracket by gluing the anterior, posterior, and lateral walls of the VF model to a corresponding cut-out in the bracket using Smooth-On Sil-Poxy. The mounting bracket had an additional cut-out posterior to the VF that enabled the insertion of five different insets. The tracheal channel spanned across both the VF and the inset in the anterior–posterior direction. Each inset had a semicircular opening that connected the subglottal and supraglottal flow channels, thereby creating an airflow bypass representative of a PGO. A photograph of the VF model and the PGO inset is presented in Figure 1c. The cross-sectional area of the semicircular openings in each inset represented half of the area of a physiological PGO and varied in size as $A_{PGO}/2$ = 0.0, 1.0, 2.5, 4.0, and 5.0 $mm^2$. In this article, we refer to the corresponding bilateral PGO area, $A_{PGO}$, which is twice the value of the size implemented in the hemilaryngeal facility, to avoid confusion. The selected PGO areas fall within the normal range of physiological PGO values (Omori et al., 1996). As shown in Figure 1c, the PGO was distinct from the VFs, separated by a distance of 1.5 mm. The center of the PGO channels was positioned 10.5 mm from the posterior surface of the VF. A PGO arises due to incomplete approximation of the arytenoid cartilages at the posterior end of the VFs. Therefore, it is not usually separated from the membranous opening of the VFs (Choi et al., 2012; Patel et al., 2012). Nevertheless, the modeling approach implemented herein is appropriate for determining how a PGO influences the VF oscillation dynamics and acoustics and is analogous to prior lumped-element PGO investigations (Zañartu et al., 2014).

The VF oscillated against a hemilaryngeal plate and was compressed medially against the plate with a static, medial prephonatory compression of 0.75 mm. This produced a medial prephonatory pressure of 1.58 kPa (see

**Figure 1.** (a) Schematic of the experimental flow facility. (b) A close-up top view of the contact plate and the relative position of the pressure sensor and the copper strip. (c) Photograph of the experimental setup without the vocal tract, showing the relative position of the vocal fold model and the posterior glottal opening. All dimensions are in millimeters.

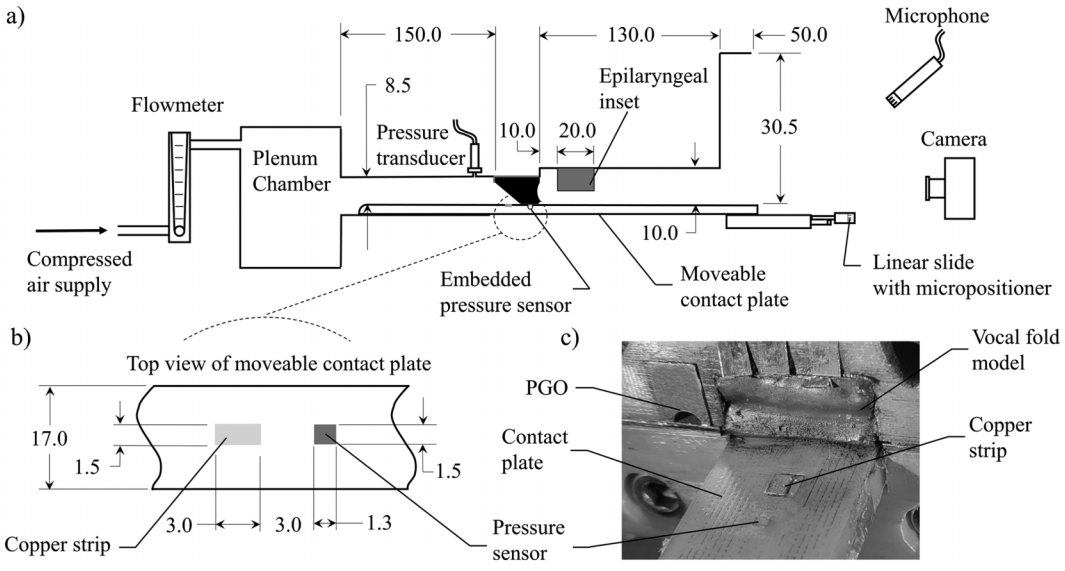

Motie-Shirazi et al., 2019, 2021a, 2021b, for the details of these measures). A Millar Mikro-Cath pressure transducer was embedded into a channel beneath the hemilaryngeal plate surface. The sensor was positioned in the channel below a 1.3 × 1.5 mm window that was filled with Smooth-On Dragon Skin 10 such that the silicone surface was flush with the surrounding contact plate. The sensing surface of the pressure transducer was positioned directly below the window. In this manner, any pressure applied to the window was directly transmitted to the sensor. A top view of the hemilaryngeal plate and the location of the contact sensor is shown in Figure 1b. The accuracy of the pressure sensor was validated by applying uniformly distributed static loads to the pressure sensor and comparing the measured pressures with ground truth values. The details of the facility and the measurement procedure can be found in prior work (Motie-Shirazi et al., 2019).

The hemilaryngeal plate was inferiorly connected to a Thorlabs PT1 linear slide that adjusted the plate's location and, therefore, the embedded contact sensor, with a precision of 0.0254 mm in the inferior–superior direction. To determine the precise position of VF collision, a copper strip was positioned at a distance of 3.0 mm inferior to the contact pressure sensor (see Figure 1b). This copper strip comprised part of a Wheatstone Bridge circuit that was also connected to the VF. The silicone VF was covered with electrically conductive graphite powder so that when the VF contacted the copper plate, a notable change in resistance through the Wheatstone Bridge was observed (Syndergaard et al., 2017). Using this approach, the precise locations of the inferior and superior edges of the VF during collision were identified by moving the contact plate in these same directions and observing the change in circuit resistance. With the known distance between the copper plate and the pressure sensor, the precise location of the pressure measurement relative to the inferior and superior edges of the VF during collision could be determined. The details of this procedure are similarly found in prior work (Motie-Shirazi et al., 2019).

A supraglottal vocal tract was 3D printed with polylactic acid plastic and placed at the exit of the VF. The surpraglottal vocal tract was a simplified model of previously reported human vocal tract geometry (Story, 2008) during the production of the vowel /a/. The vocal tract had a constant length of 26.2 mm in the anterior–posterior direction and consisted of two connected sections with discrete cross-sectional areas. The inferior section had a medial–lateral width of 10.0 mm and an inferior–superior height of 130.0 mm, which transitioned to the superior section with a width of 30.5 mm and a height of 50.0 mm (see Figure 1a). The supraglottal compression was controlled by individually inserting three separate plastic insets of varying width inside the epilarynx tube and bolting them to the vocal tract at a distance of 10.0 mm superior to the VF exit (see Figure 1a). All three insets had an inferior–superior height of 20.0 mm and an anterior–posterior length of 26.2 mm (equal to the length of the vocal tract). The medial–lateral widths of the insets varied as 6.2, 8.4, and 9.2 mm, creating epilaryngeal areas of $A_{ep}$ = 99.6, 41.9, and 21.0 mm$^2$, respectively, which were within the range of physiological values (Döllinger et al., 2006; Story et al., 1996; Titze, 2006).

A B&K 4189 (Brüel & Kjær) microphone was placed at a distance of 150 mm from the vocal tract exit in a 45° orientation relative to the air channel to measure the acoustic pressure and calculate the radiated SPL. This microphone is suited for use in Class 1 sound-level meters and was calibrated prior to each measurement with a Rion NC-74 Class I sound calibrator (Rion Co.). High-speed video (HSV) of the VF oscillations was recorded by a Photron AX2000 high-speed camera with an Elicar V-HQ Macro 90 mm f 2:5 lens (Jaca Corporation), positioned superior to the VF. The HSV was recorded at 80,000 frames per second at a spatial resolution of 0.088 mm/pixel. The entire facility was located inside an acoustic booth to minimize ambient noise. The A-weighted background SPL was measured to be 33 dBA inside the acoustic booth.

The unsteady subglottal, collision, and acoustic pressure data were acquired with a National Instruments PCIe-6321 data acquisition card and a custom LabVIEW program. The sampling rate was 80 kHz, and the data were collected for a duration of 0.75 s.

## Vocal Fold Model

The VF model consisted of four layers of adipose tissue, body, cover, and epithelium. The details of each layer and the fabrication process can be found in the study of Motie-Shirazi et al. (2019). Figure 2 displays a schematic of the coronal cross-section of the model. It has been shown that inclusion of the adipose tissue, a fatty layer that fills the paraglottic space (Reidenbach, 1996), in

**Figure 2.** Geometry and key dimensions of the synthetic vocal fold model. All dimensions are in millimeters.

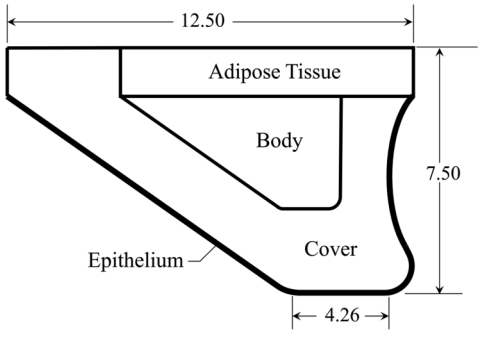

VF models improves VF oscillations by reducing the fundamental frequency (Jones et al., 2015; Wu & Zhang, 2021). The anterior–posterior length of the model was 17 mm. The magnitude of the complex modulus of elasticity of each layer and the corresponding physiological range are presented in Table 1, showing that the measured silicone moduli were physiologically relevant. Note that although the silicone mixture ratios used for the fabrication of each layer were the same as those used in prior studies (Motie-Shirazi et al., 2021a, 2021b), the moduli of elasticity were slightly different. This variation arises because the material properties of the silicone rubber can vary across different batches and depends on local environmental conditions such as humidity and temperature during the casting process.

## Experimental Procedure

To investigate the influence of compensatory behaviors, the subglottal pressure, $p_{sub}$, was adjusted to reach a reference SPL value of 88.0 dB SPL, in which persistent VF oscillations were obtained for all of the cases that were studied. First, the influence of PGO size was studied by inserting the five different PGO insets individually, under the condition of no supraglottal compression. For each case, the inferior and superior margins of the collision region at the anterior–posterior midline were determined. The unsteady collision pressure data were then collected by moving the pressure sensor in the inferior–superior direction within the collision region in increments of 0.254 mm.

In addition, for each condition, the magnitude of the VF surface velocity immediately preceding collision, $V_c$, was calculated based on HSV recordings of the VF oscillation, which is a commonly accepted approach in extracting the VF kinematics in clinical and synthetic VF investigations (DeJonckere & Lebacq, 2020; Murray & Thomson, 2012). To accomplish this, a threshold value of the pixel brightness intensity was defined to discern the medial edge of the VF in each frame of the video, thereby tracking its movement. The collision velocity, $V_c$, was specified as the average velocity of the medial edge of the VF as it traversed the last three pixels in the medial–lateral direction before impacting the contact plate. This distance was 0.264 mm, which took about 0.25 ms (i.e., 20 frames of the video) to traverse. Because the window that connected the embedded pressure sensor to the hemilaryngeal plate at the anterior–posterior midline had an anterior–posterior length of 1.5 mm (see Figure 1b), the collision velocity was calculated over this same range of anterior–posterior locations and then averaged to find the mean VF collision velocity. The collision pressure data, together with the VF collision velocity, were used to compute the dissipated power of the VF during collision using the method initially proposed by Titze and Hunter (2015) and subsequently refined in the study of Motie-Shirazi et al. (2021a). This method is briefly reviewed in the Dissipated Power Dose Analysis section.

In the second set of experiments, the three epilaryngeal insets were independently added to the supraglottal vocal tract, and the experiments were repeated by changing the PGO area and adjusting the subglottal pressure, $p_{sub}$, to reach an SPL of 88.0 dB SPL at 150.0 mm. The zone of VF collision was identified for each case, and the collision pressure was recorded. Because insertion of the epilaryngeal insets obscured the camera viewpoint, visualization of the VF oscillations could not be recorded for these cases.

It should be noted that in similar numerical studies (Galindo et al., 2017; Zañartu et al., 2014; Zhang, 2021), the compensation procedure aimed to compare the influence of different PGO sizes and epilaryngeal areas on the collision dynamics of the VFs by maintaining a constant vocal intensity (i.e., SPL). This approach allows for direct comparison, but it does not consider the importance of the excess pressure over the threshold pressure, which has been proposed as an important factor affecting vocal intensity (Titze & Sundberg, 1998). Nevertheless, it does quantify how compensatory efforts to achieve a constant SPL likely lead to phonotrauma.

## Dissipated Power Dose Analysis

The total dissipated power of the VFs during collision, which is a combination of the dissipated power due to internal friction and collision, has been suggested as a measure of phonotraumatic VF damage (Titze & Hunter, 2015; Titze et al., 2003). Prior work has shown that the

**Table 1.** Moduli of elasticity of physiological and silicone vocal fold models for each layer.

| Layer | Physiological range (kPa) | Silicone vocal fold model (kPa) |
|---|---|---|
| Adipose tissue | 1–10 (Comley & Fleck, 2012) | 4.85 |
| Body | 1.5–50 (Chhetri et al., 2011; Dion et al., 2017; Min et al., 1995) | 8.37 |
| Cover | 1–8 (Alipour & Vigmostad, 2012; Chan et al., 2007; Chan & Rodriguez, 2008; Chan & Titze, 1999; Chhetri et al., 2011; Oren et al., 2014) | 1.31 |
| Epithelium | Not measured | 75.43 |

dissipated collision power is an order of magnitude greater than the dissipated frictional power and, consequently, is likely the primary cause of VF injury (Motie-Shirazi et al., 2021a). Moreover, it has been observed that the dissipated power has the highest magnitude at the anterior–posterior midline (Motie-Shirazi et al., 2021a), where VF lesions are normally formed (Dikkers & Nikkels, 1999). Therefore, dissipated collision power was only measured along the anterior–posterior midline in this study. A short review of the method developed in the prior work (Motie-Shirazi et al., 2021a) to calculate the dissipated power during VF collision is presented below.

Based on an energy budget analysis, the dissipated energy during collision ($W_d$) can be expressed as the total energy of the VF prior to collision, which is the difference between the kinetic energy ($W_k$) and the elastic energy restored to the VF at the end of collision when the VF stops moving ($W_c$). Dividing these values by the period of VF oscillation ($T$) and the volume ($V$) of the VF, the equation for dissipated power per unit volume, $\dot{W}_d$, is obtained as

$$\dot{W}_d = \dot{W}_k - \dot{W}_c \tag{1}$$

where $\dot{W}_k$ is the kinetic power and $\dot{W}_c$ is the collision power. These values are defined on a per-unit VF volume basis. However, for brevity, they will be referred to by their fundamental units for the remainder of the article. It should be noted that it is inappropriate to calculate the dissipated power as the difference between the kinetic power of the VF before and after collision because aerodynamic power is still applied to the VF during the closed portion of the vibratory cycle. This has the effect of increasing the velocity at which the VFs open following collision.

The kinetic power, $\dot{W}_k$, was estimated by approximating the velocity profile inside the VF. It has been shown that the cover layer experiences a higher deformation than the body layer during VF oscillation (Mendelsohn et al., 2007). However, the internal displacement and velocity magnitudes have not been evaluated. Approximating the VF geometry as a trapezoid, with a medial surface velocity of $V_c$ immediately preceding collision, and assuming that the velocity within the VF quadratically decreases to zero at the lateral surface yield

$$\dot{W}_k \approx \frac{0.06}{T}\rho V_c^2, \tag{2}$$

where $\rho \approx 1{,}040$ kg/m$^3$ is the average density of the VF and $T$ is the period of oscillation.

The collision power, $\dot{W}_c$, was computed as the work done on the VF by the average collision force divided by the VF volume and period of oscillation. This gives $\dot{W}_c \approx \left(F_{c,avg}\,\delta_c\right)/(VT)$, where $\delta_c$ is the fictitious penetration depth of the VF during collision, which could not be measured directly and is therefore approximated by assuming a Hertzian model of contact. Subsequently, the collision power at the mid coronal plane of the VF can be written based on the average collision pressure as

$$\dot{W}_c \approx \frac{p_{c,avg}\, l_c\, \delta_c}{A\, T}, \tag{3}$$

where $p_{c,avg}$ is the temporal and spatial average of the collision pressure, $l_c$ is the inferior–superior thickness of contact during collision, and $A$ is the coronal cross-sectional area of the VF. The Hertzian contact model correlates the deformation during collision to the resultant collision pressure, the geometrical shape of the body, and its material properties. To estimate $\delta_c$, a Hertzian model of contact between two identical cylinders was employed (Díaz-Cádiz et al., 2019). The accuracy of this method has been validated previously by obtaining the fictitious penetration depth from HSV of VF oscillations and comparing the value of the peak collision pressure predicted by the Hertzian model with the actual value measured with a pressure sensor (Díaz-Cádiz et al., 2019; Mehta et al., 2021). Using this approach, the maximum collision pressure, $p_{c,max}$, is given by

$$\frac{p_{c,max}}{E^*} = 4\frac{\delta_c}{l_c}, \tag{4}$$

where $E^* = E/[2(1 - v^2)]$ is the effective Young's modulus of the VF, $E$ is the equivalent Young's modulus of the layered VF structure, and $v$ is Poisson's ratio. Because the VF model comprises multiple layers with different material properties, the equivalent value of $E$ cannot be measured directly. Therefore, the effective Young's modulus, $E^*$, was estimated by utilizing the proposed Hertzian contact model but applying it to the prephonatory condition of the VF. The VF had a medial–lateral length of 7.50 mm and an inferior–superior thickness of 4.26 mm. Approximating the VF as a deformed trapezoid that was compressed medially by a distance of 0.75 mm results in a medial thickness of 6.12 mm in the prephonatory condition. Substituting these prephonatory values into Equation 4 yields a value of $E^* = 4.93$ kPa. The computation details for this technique can be found in the study of Motie-Shirazi et al. (2021a).

The proposed Hertzian contact model approximates the penetration depth of the VF tissue during collision by assuming contact between two elastic cylinders with the axial coordinate along the anterior–posterior direction. Therefore, the Hertzian model does not include the viscoelastic properties of the VF tissue. Nevertheless, it has been shown that this method provides reasonable approximations of the VF collision pressure (Díaz-Cádiz et al., 2019; Mehta et al., 2021). In addition, it has been shown that the VF tissue coefficient of restitution predicted with this method is consistent with physiological values (Motie-Shirazi et al., 2021a). This

suggests that the employed model provides reasonable approximations of the VF penetration depth and dissipated collision power. More precise calculations of the dissipated collision power may be achieved by directly measuring internal VF stress and strain fields, which would enable implementation of material damping models. Although these efforts are a focus of ongoing work, they are beyond the scope of this study.

## Results

### VF Dynamics

The key oscillation features of the VF model were first compared to physiological values. The onset pressure, $p_{onset}$, with no PGO and no supraglottal compression was measured to be 1.72 kPa. The radiated SPL at the phonation onset pressure, $SPL_{onset}$, was 81.7 dB SPL. To produce the target SPL of 88.0 dB SPL, the subglottal pressure, $p_{sub}$, was increased to 2.53 kPa. This produced a mean flow rate of $Q$ = 585 ml/s and a fundamental frequency of $f_o$ = 149 Hz. Although the acoustic and aerodynamic measures fall within the range of physiological values, the onset pressure is abnormally high. This can be attributed, in part, to the hemilaryngeal configuration, which is known to increase onset pressure (Jiang & Titze, 1994; Mehta et al., 2019; Murray & Thomson, 2012). In addition, the application of prephonatory compression of the VF with the medial wall, which was applied to ensure robust collision during oscillation, also increased the onset pressure. At the mid anterior–posterior location, the open quotient, the ratio of time that the VF is open to the period of one oscillation cycle, was 0.71, and the speed quotient, the ratio of the time of the opening phase to the closing phase, was 2.03. These values fall within normal physiological ranges (Kania et al., 2004; Lohscheller et al., 2013). For $p_{sub}$ = 2.53 kPa, the maximum medial–lateral glottal distance at the midline and the maximum glottal hemilaryngeal area were 1.05 mm and 13.71 $mm^2$, respectively, which are also representative of human VF values (Döllinger & Berry, 2006; Titze & Alipour, 2006). These findings indicate that although the onset pressure was high, the resultant VF kinematics and dynamics are physiologically relevant.

### Influence of a PGO

The dynamics of the VF oscillation were initially investigated as a function of the posterior glottal area, $A_{PGO}$, for the situation of no supraglottal compression ($A_{ep}$ = 262.0 $mm^2$). Figure 3 presents the change in the onset pressure, $p_{onset}$, and SPL at onset, $SPL_{onset}$, as a function of PGO area, $A_{PGO}$. Note that all the plots presented in this study display different parameter magnitudes at five discrete PGO areas, and the dashed lines connecting the symbols have been added for better visualization of the trends. A monotonically increasing trend is generally observed for both. The value of SPL at onset corresponds to the ability to produce low-intensity voice as the PGO area increases. Similar behavior has been observed using a computational model of the VFs (Zhang, 2019).

**Figure 3.** Onset pressure, $p_{onset}$ (square markers, left axis), and onset sound pressure level, $SPL_{onset}$ (circle markers, right axis), as a function of posterior glottal opening area. The markers denote the mean value, and the error bars indicate the maximum and minimum values.

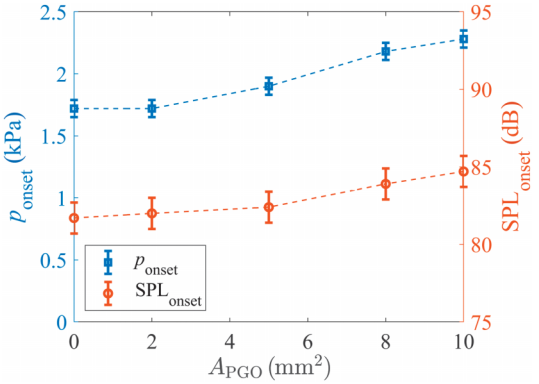


The effect of the PGO area on the SPL was investigated for a fixed subglottal pressure of $p_{sub}$ = 2.53 kPa. As shown in Figure 4, the SPL initially increased for the smallest PGO area ($A_{PGO}$ = 2 $mm^2$) and then decreased linearly with increasing PGO area. This finding was in agreement with previous numerical studies (Galindo et al., 2017) that demonstrated that the SPL actually achieved a local maximum for a very small PGO area. It has

**Figure 4.** Sound pressure level (SPL) as a function of posterior glottal opening area, $A_{PGO}$, at a constant subglottal pressure of 2.53 kPa. The markers denote the mean value, and the error bars indicate the maximum and minimum values.

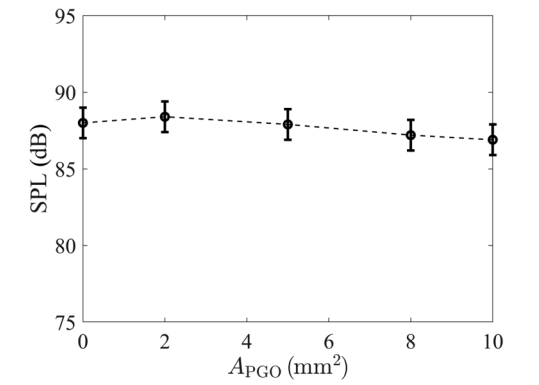

similarly been argued that maintaining a small glottal opening is actually beneficial for normal voice production (Zhang, 2015). Note that the observed SPL variations were within the range of the 1-dB uncertainty of the microphone, as shown by the error bars in Figure 4. The identifiable trend in SPL as a function of PGO area, however, suggests that the microphone was able to reliably capture the small SPL variations in this range. Regardless, the microphone uncertainty is a clear limitation that could be improved in future studies.

The radiated SPL was 1.1 dB lower for $A_{PGO}$ = 10.0 mm$^2$ than for the case with no PGO. This reduction was significantly less than the decrease of about 15 dB that was reported in lumped-element model investigations (Galindo et al., 2017; Zañartu et al., 2014). Clinical studies have reported a decrease of 3.7 dB at maximum phonation intensity when a PGO exists (Schneider & Bigenzahn, 2003), although this difference was not correlated with PGO size. These discrepancies likely arise from the strength of the acoustic loading effects, which can be estimated by determining the acoustic gain of the vocal tract at the resonance frequency. The resonance frequency and the acoustic gain of the current physical vocal tract model were found by using a loudspeaker at the entrance of the vocal tract and measuring the acoustic pressure at the vocal tract exit. The first resonance frequency was found to be at 660 Hz, close to the first formant frequency of 750 Hz for the vowel /a/ in male voice (Catford, 1988). The power gain at this frequency was 7.8 dB. In the lumped-element investigations (Galindo et al., 2017; Zañartu et al., 2014), the acoustic gain value for the vocal tract model of vowel /e/, which has a first formant of approximately 390 Hz, was computed to be around 20 dB. Clinical studies have measured a 10–15 dB power gain at the first formant of the human vocal tract (Harrison, 2013; Sundberg, 1988). The lower value of the acoustic gain in the current work, particularly with respect to the prior lumped-element model investigations, indicates that the influence of acoustic loading effects may be diminished. In addition, the first formant frequency, relative to the fundamental frequency of VF oscillation, is much higher for the supraglottal tract orientation representative of /a/ than it is for /e/, which will further reduce the impact of acoustic loading. Nevertheless, the physics of the fluid–structure–acoustic interactions is captured, which enables investigation of the main study objective, namely, determining how measures of collision pressure and dissipated collision power vary as a function of PGO size.

Similar to previously employed approaches (Galindo et al., 2017; Zañartu et al., 2014), compensation for the decreased SPL was performed by adjusting the subglottal pressure to achieve the target SPL (88.0 dB), which was recorded for a PGO area of $A_{PGO}$ = 0.0 mm$^2$ at a subglottal pressure of $p_{sub}$ = 2.53 kPa. The compensated subglottal pressure, $p_{sub}$, and the associated peak collision pressure at the anterior–posterior midline, $p_{c,\,max}$, are plotted in Figure 5a. The latter is reported as the maximum collision pressure that occurred in the inferior–superior direction at the anterior–posterior midline. The reported mean values denote the average pressure magnitudes over all of the oscillation cycles recorded during the 0.75-s data

**Figure 5.** The (a) subglottal pressure ($p_{sub}$) and peak collision pressure ($p_{c,max}$), (b) mean flow rate ($Q$), and (c) fundamental frequency ($f_o$) as a function of posterior glottal opening area, where the subglottal pressure was adjusted (i.e., compensated) to achieve a target sound pressure level of 88.0 dB SPL. The markers denote the mean value, and the error bars indicate the maximum and minimum values.

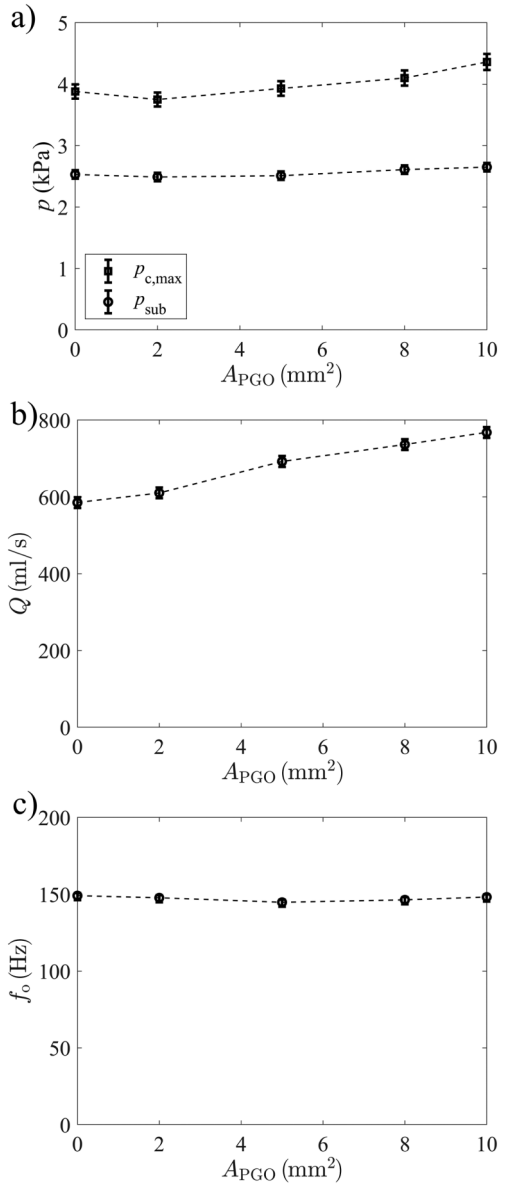

collection interval, and the error bars indicate a combination of the variation in the measured values over the recorded cycles and the error of the measuring device.

The subglottal pressure required to achieve the reference SPL was the lowest for $A_{PGO}$ = 2.0 mm$^2$ and then increased, reaching a maximum value for $A_{PGO}$ = 10 mm$^2$, as shown in Figure 5a. A similar trend was observed for the peak collision pressure, $p_{c,max}$. Interestingly, although the subglottal pressure had a modest increase of 5% as the PGO area increased to $A_{PGO}$ = 10.0 mm$^2$, a more notable rise of 12% was observed for the peak collision pressure. Although this increase was substantial, it was not as pronounced as that predicted by lumped-element model investigations (Galindo et al., 2017; Zañartu et al., 2014), which reported up to a 100% increase in the collision force for a PGO of $A_{PGO}$ = 10 mm$^2$.

As displayed in Figure 5b, increasing the PGO area resulted in higher mean flow rates, with a 31% increase observed for the largest PGO when subglottal pressure compensation was performed to maintain the target SPL. Unfortunately, the measurement limitations precluded distinguishing the AC and DC components of the flow. Only a minor fluctuation of 4 Hz was observed in the fundamental frequency (see Figure 5c).

## Computing Dissipated Collision Power

Using the method introduced in the Dissipated Power Dose Analysis section, the dissipated collision power was also calculated as a function of PGO for the case where the subglottal pressure was adjusted to achieve the target SPL value of 88 dB. To compute the dissipated collision power, the kinetic power, $\dot{W}_k$, was first calculated using Equation 2. This required estimating the magnitude of the VF collision velocity, $V_c$, for each case. The velocity magnitudes and the associated errors are presented in Figure 6a. Note that preceding closure, the visible medial boundary corresponded to the inferior edge of the VF. Therefore, the reported collision velocities present the velocity of the inferior VF edge.

An increase in the mean collision velocity, $V_c$, is observed for increasing PGO area. For the largest PGO area of $A_{PGO}$ = 10 mm$^2$, compensating to maintain the target SPL created a 13% larger glottal area, which, on average, resulted in a 20% increase in the collision

**Figure 6.** The (a) collision velocity; (b) spatially averaged collision pressure; (c) kinetic (diamond), collision (triangle), and dissipated (circle) powers; and (d) dissipation coefficient, as a function of posterior glottal opening area. Compensation to maintain the target sound pressure level of 88 dB SPL was achieved by adjusting the subglottal pressure. The markers denote the mean value, and the error bars indicate the maximum and minimum values.

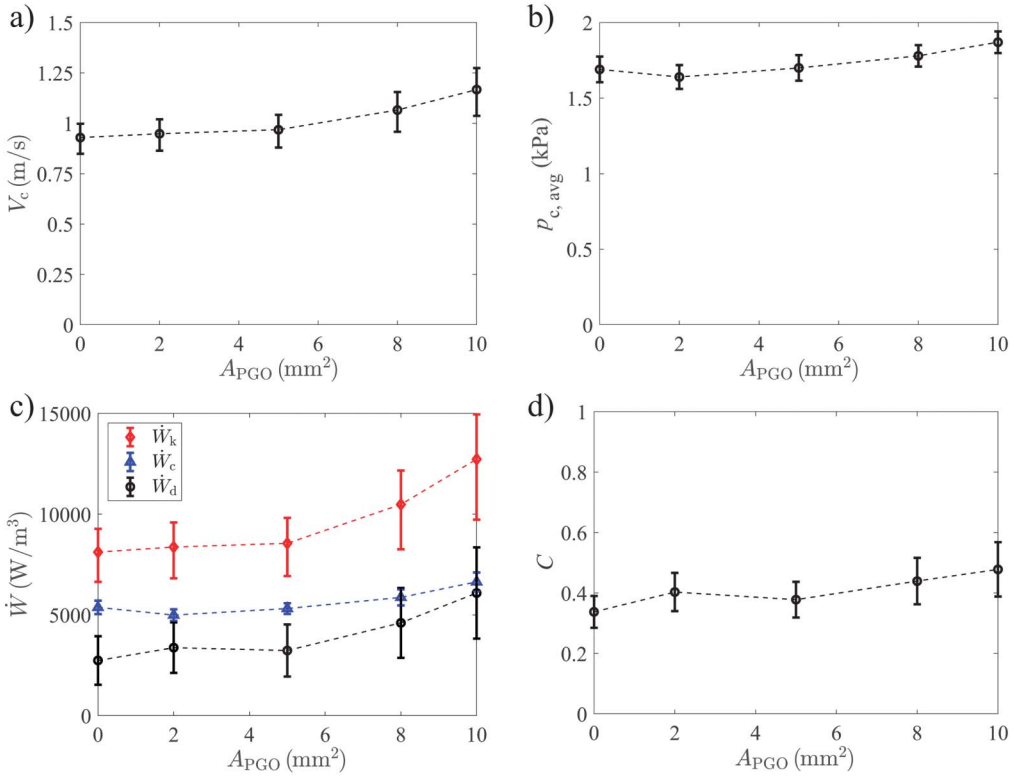

velocity. Prior in vivo investigations have similarly observed that collision velocity is highly correlated with subglottal pressure and radiated SPL (DeJonckere & Lebacq, 2020). The collision velocity values were then used to compute the kinetic power, $\dot{W}_k$, for each of the PGO areas. For kinetic power calculations, the VF surface velocity is assumed to be constant along the inferior–superior direction and equal to the velocity of the inferior edge. Note that due to the experimental limitations, computing the velocity from the HSV recordings resulted in roughly 10% error, as shown in Figure 6a. A higher frame rate and/or spatial resolution is needed to decrease the uncertainty of these measurements, which is a focus of ongoing efforts.

For each PGO size, the average collision pressure, $p_{c,avg}$, was computed along the anterior–posterior midline by spatiotemporally averaging the collision pressure over the inferior–superior collision thickness, throughout the collision period. The values are presented in Figure 6b. A 10% rise in the average collision pressure was observed for the largest PGO area, which was higher than the increase in the subglottal pressure but less than for the peak collision pressure. For all of the PGO areas, the collision thickness, $l_c$, remained largely constant at 2.75 mm. The values of maximum collision pressure, collision thickness, and effective Young's modulus were used to compute the penetration distance, $\delta_c$, from Equation 4. Equation 3 was then used to calculate the collision power, $\dot{W}_c$, as a function of PGO area.

Finally, the dissipated power, $\dot{W}_d$, was calculated as the difference between the kinetic and collision power (Equation 1). The variation of the kinetic, collision, and dissipated powers is displayed as a function of PGO area in Figure 6c. Note that the power magnitudes presented in this figure satisfy the power balance of $\dot{W}_d = \dot{W}_k - \dot{W}_c$. The mean value of the dissipated power increased as the PGO area increased. Interestingly, although the increase in the peak collision pressure, $p_{c,max}$, was only 12% for the PGO area of $A_{PGO}$ = 10.0 mm$^2$ (see Figure 5a), the dissipated power, $\dot{W}_d$, increased by 122% on average. This deviation from the more modest variation exhibited by the peak collision pressure as a function of PGO area is because the dissipated collision power is derived from the collision pressure and the squared VF collision velocity, which also increased with PGO area. This is an important new finding, as dissipated power during collision is believed to be a more accurate predictor of phonotrauma. It predicts that, with increasing PGO area, the potential for phonotrauma is greatly increased and that this risk may not be adequately captured by only considering the peak collision pressure.

It should be noted that the uncertainty in the computed dissipated power was around 40% due to the relatively high error in the estimation of the collision velocity. Nevertheless, a clear nonlinear increase in the mean dissipated power is evident. Figure 6d presents the computed dissipation coefficient, $C$, defined as the ratio of dissipated to kinetic power ($C = \dot{W}_d/\dot{W}_k$). Prior work for a single phonatory condition reported a value of $C$ = 0.52 (Motie-Shirazi et al., 2021a), resulting in a coefficient of restitution of $e \approx 0.69$, which was found to fall within the range of similar biological tissues ($e \approx$ 0.4–0.76; Anderson et al., 2014; Edelsten et al., 2010). In this study, compensating for the 1.1-dB reduction in SPL resulted in a 41% increase in the dissipation coefficient for a PGO area of $A_{PGO}$ = 10.0 mm$^2$, indicating that as PGO area increases, a greater portion of the kinetic power is dissipated during VF collision. This is also a useful finding as it expands upon prior work to show that patient-specific dissipation coefficients can be expected to vary as a function of physiological and phonatory conditions.

## Influence of Supraglottal Compression

The influence of supraglottal compression on the collision dynamics was explored following the method described in the Experimental Procedure section. The studied epilaryngeal areas were $A_{ep}$ = 21.0, 41.9, 99.6, and 262.0 mm$^2$, giving ratios of epilaryngeal area to maximum bilateral glottal area of 0.77, 1.53, 3.63, and 9.56, respectively. Figure 7a presents the subglottal pressure, $p_{sub}$, required to maintain the target SPL of 88.0 dB as a function of epilaryngeal and PGO area. The trend in subglottal pressure versus PGO area was very similar to that of the nonconstricted vocal tract with a PGO area of $A_{ep}$ = 262.0 mm$^2$ (shown in Figure 5a). The magnitude of the subglottal pressure was lowest for $A_{PGO}$ = 2.0 mm$^2$ and then increased as the PGO area increased. The rise in the subglottal pressure was a modest 3%–5% across all epilaryngeal areas.

Interestingly, as shown in Figure 7a, as the epilaryngeal area decreased from $A_{ep}$ = 262.0 mm$^2$ to $A_{ep}$ = 99.6 mm$^2$, the subglottal pressure needed to reach the target SPL actually decreased by about 4%. That is, as the epilaryngeal area decreased, the SPL showed a modest increase. Further reduction in the epilaryngeal area to $A_{ep}$ = 41.9 mm$^2$ and $A_{ep}$ = 21.0 mm$^2$ increased the subglottal pressure needed to reach the target SPL. This is in agreement with prior lumped-element model investigations (Galindo et al., 2017) that showed that the supraglottal compression has an optimum value that maximizes SPL. However, this finding contradicts the results obtained from a three-dimensional computational modeling that found the SPL continuously increased with epilaryngeal narrowing (Zhang, 2021).

Similar to the subglottal pressure, the peak collision pressure, $p_{c,max}$, had the lowest magnitude for an

**Figure 7.** The (a) subglottal pressure ($p_{sub}$) and (b) peak collision pressure ($p_{c,\,max}$) for different epilaryngeal areas ($A_{ep}$) as a function of posterior glottal opening area ($A_{PGO}$) when compensating to achieve a target sound pressure level of 88.0 dB.

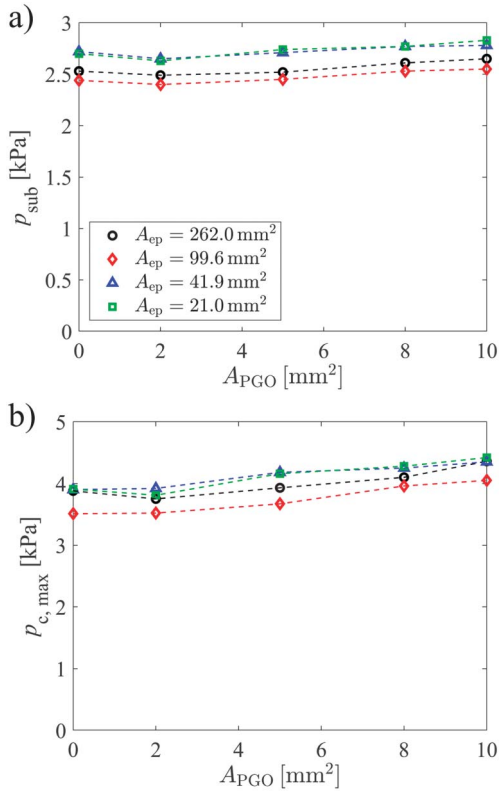


epilaryngeal area of $A_{ep}$ = 99.6 mm$^2$ (as shown in Figure 7b). On average, the variation in the peak collision pressure as a function of epilaryngeal area was around 9%. In addition, variation of the peak collision pressure versus PGO area for the constricted configurations exhibited similar trends to the case with no supraglottal compression. In all cases, the peak collision pressure increased by 11%–15% for the largest PGO area when compared to zero PGO area.

Unfortunately, the collision velocity and, consequently, the dissipated power could not be obtained in the investigations with the supraglottal compression due to lack of optical access. However, based on similar behaviors of the peak collision pressure and the dissipated power observed for the nonconstricted epilarynx discussed in the Influence of a PGO section, it can be reasonably concluded that the dissipated power will likely be the lowest for an epilaryngeal area of $A_{ep}$ = 99.6 mm$^2$. If true, this would indicate that constricting the epilarynx to achieve an optimal level of constriction and thereby maximize SPL could be an effective compensatory behavior that avoids the destructive effects of compensating for increased PGO area by increasing the subglottal pressure.

## Discussion

It is believed that compensatory behaviors due to the presence of a PGO can contribute to chronic tissue trauma, where further phonatory compensations in the presence of the resultant pathology exacerbate the problem and create a deleterious cycle of VF damage (Hillman et al., 1989, 2020). However, the mechanism by which compensation causes phonotraumatic VF damage is not well understood. This study provides new insights into the pathophysiology of VF trauma resulting from compensatory behaviors. An important advantage of the method used in this study was that it facilitated investigation of not only the peak collision pressure, which is commonly used as a precursor for predicting VF damage, but also the spatial variation of the collision pressure over the collision thickness. Resolving the spatial distribution of the collision pressure enabled computation of the power that is dissipated during VF collision.

The most interesting observation of this work was that although modest increases in collision pressure were observed with increasing PGO area, the dissipated collision power exhibited a much more marked and nonlinear increase. For the largest PGO area, the peak collision pressure increased by 12%, whereas the corresponding dissipated collision power increased by 122%. This finding is important because the dissipated power, which is manifest as thermal energy inside the VF, is believed to be a more accurate predictor of phonotrauma that will likely lead to the formation of benign VF lesions (Gray & Titze, 1988; Rousseau et al., 2011; Zhao et al., 1991).

These findings also indicate that peak VF collision pressure may not, by itself, be an adequate measure for predicting phonotrauma. This is evidenced by noting that, in this study, the peak collision pressure initially decreased with increasing PGO area (see Figure 5a), suggesting that a small amount of PGO may be beneficial for sound production. This observation has similarly been reported in prior work (Galindo et al., 2017). However, inspection of Figure 6c reveals that the dissipated power consistently increases with increasing PGO area. The reason is that although the peak collision pressure initially decreases with increasing PGO area, the collision velocity increases (see Figure 6a), which results in a higher dissipated power. Therefore, although a small PGO area appears to boost the SPL, the dissipated collision power still increases, thereby theoretically increasing the potential for phonotrauma. However, the thresholds at which dissipated collision power begins to cause VF tissue damage are unknown. Thus, the small increase in dissipated collision power due to a small PGO area that optimizes SPL may fall within safe limits. This is supported by common observations of small PGOs in vocally healthy speakers (Cielo et al.,

2019; Linville, 1992; Patel et al., 2012; Schneider & Bigenzahn, 2003).

Noting the importance of dissipated power as a predictor of phonotrauma may also help explain the high prevalence of benign VF lesions in women. Namely, the increased prevalence of a PGO (Hanson, 1997; Linville, 1992), in tandem with the higher VF velocities that naturally occur due to higher fundamental frequencies, gives rise to an environment that is more likely to support higher values of dissipated collision power.

Patients with phonotraumatic VF lesions are often advised to reduce their loudness (Holmberg et al., 2001), which is indirectly supported by the results of this investigation, which showed that efforts to compensate for even a small 1.1-dB drop in vocal intensity resulted in a 122% increase in the dissipated power (see Figure 6c). Thus, tolerating a lower vocal SPL would be expected to prevent a large increase in dissipated collision power and thereby reduce the potential for continued phonotrauma.

It was discovered that although reducing the epilaryngeal area did not have a significant influence on the radiated SPL, some degree of compression can be beneficial to compensate for the reduced SPL when a PGO was present. The SPL achieved a local maximum for an epilaryngeal area of $A_{ep}$ = 99.6 mm$^2$. As a result, a lower subglottal pressure was required to produce the same SPL as the nonconstricted condition, which also reduced the peak collision pressure (as shown in Figure 7b). Although this was consistent with prior observations (Galindo et al., 2017), care should be taken in interpreting these results because the corresponding VF collision velocity, which is a key measure in computing the dissipated power, was not able to be determined due to the lack of optical access. Therefore, the variation of dissipated collision power with the epilaryngeal area could not be studied to investigate if it also shows a similar trend as the peak collision pressure. In addition, investigating these behaviors using a smaller increment in epilaryngeal areas would provide a more accurate estimation of an optimal area.

The measured decrease in SPL as a function of PGO area was consistent with computational investigations (Zhang, 2016), but it was significantly lower than that predicted via lumped-element models (Zañartu et al., 2014), whereas clinical measures fall in between the two (Schneider & Bigenzahn, 2003). This discrepancy likely arises from differences in how the supraglottal tract and associated acoustic loading effects are modeled.

Finally, it should be taken into account that these results have been obtained by performing investigations with a synthetic VF model in a hemilaryngeal facility, which is not without limitations. Although it was shown that the synthetic models produce physiologically relevant oscillation kinematics, these models suffer from higher-than-normal phonation threshold pressure. Therefore, the study was conducted with subglottal pressures that were higher than the normal range of speech. Although it is expected that this does not influence the overall trends of the collision dynamics, the resultant magnitudes and their ratios might change at lower subglottal pressures. Another source of error was the measurement uncertainty of the microphone, which was greater than some of the measured variations in SPL. Therefore, care should be taken when interpreting the results. Nevertheless, an identifiable pattern of decreasing SPL with increasing PGO size was observed for all cases. In addition, various assumptions were employed to compute the dissipated collision power. First, a Hertzian contact model was utilized to estimate the fictitious penetration depth of the VF, which does not consider the viscoelastic properties of the material. Second, the VF surface velocity, which was used to compute the kinetic power of the VF, was considered to be constant in the inferior–superior direction. Lastly, the kinetic power was estimated based on the assumption that the velocity decreases quadratically inside the VF tissue. More accurate magnitudes of penetration depth and kinetic power can be achieved by measuring the displacement and velocity fields inside the VF tissue, which is the subject of ongoing work.

## Conclusions

Abnormally high peak collision pressure and dissipated collision power of the VFs have been considered as the main contributors to the emergence of phonotrauma and the subsequent formation of benign lesions. The phonotraumatic effect of a PGO on these two measures of damage was investigated by employing synthetic silicone models of the VFs in a hemilaryngeal setup. Although both the peak collision pressure and dissipated collision power increased nonlinearly as a function of the PGO area, the peak collision pressure increased by 12% for the largest PGO area of 10.0 mm$^2$, whereas the dissipated collision power increased by 122%. These results indicate that dissipated collision power may be a more accurate predictor of phonotrauma than peak VF collision pressure. It was also shown that, acoustically, there is an optimal degree of supraglottal compression that increases the radiated SPL. However, drastic narrowing of the epilarynx created an adverse effect, reducing the SPL and increasing the resultant peak collision pressure. The influence of supraglottal compression on dissipated collision power remains a subject of future work. Finally, the uncertainty of the SPL measurements, which was higher than some of the observed variations in the SPL measurements, was one of the limitations of this study. Improving the microphone accuracy in future investigations would enable more reliable interpretations of the results.

## Author Contributions

**Mohsen Motie-Shirazi:** Conceptualization (Equal), Formal analysis (Lead), Investigation (Equal), Methodology (Equal), Writing – original draft (Lead), Writing – review & editing (Equal). **Matías Zañartu:** Conceptualization (Supporting), Funding acquisition (Lead), Investigation (Supporting), Methodology (Supporting), Supervision (Supporting), Writing – original draft (Supporting), Writing – review & editing (Supporting). **Sean D. Peterson:** Conceptualization (Supporting), Formal analysis (Supporting), Funding acquisition (Supporting), Investigation (Supporting), Supervision (Supporting), Writing – original draft (Supporting), Writing – review & editing (Supporting). **Daryush D. Mehta:** Conceptualization (Supporting), Funding acquisition (Equal), Writing – original draft (Supporting), Writing – review & editing (Supporting). **Robert E. Hillman:** Conceptualization (Supporting), Funding acquisition (Lead), Writing – original draft (Supporting), Writing – review & editing (Supporting). **Byron D. Erath:** Conceptualization (Lead), Formal analysis (Lead), Funding acquisition (Supporting), Investigation (Lead), Methodology (Lead), Project administration (Lead), Supervision (Lead), Writing – original draft (Equal), Writing – review & editing (Equal).

## Acknowledgments

This research was supported by National Institute on Deafness and Other Communication Disorders Grant P50 DC015446 (PI: Hillman) and ANID BASAL FB0008 (PI: Zañartu). The content is solely the responsibility of the authors and does not necessarily represent the official views of the National Institutes of Health.

## References

**Åkerlund, L., & Gramming, P.** (1994). Average loudness level, mean fundamental frequency, and subglottal pressure: Comparison between female singers and nonsingers. *Journal of Voice, 8*(3), 263–270. https://doi.org/10.1016/S0892-1997(05)80298-X

**Alipour, F., Jaiswal, S., & Finnegan, E.** (2007). Aerodynamic and acoustic effects of false vocal folds and epiglottis in excised larynx models. *Annals of Otology, Rhinology & Laryngology, 116*(2), 135–144. https://doi.org/10.1177/000348940711600210

**Alipour, F., & Vigmostad, S.** (2012). Measurement of vocal folds elastic properties for continuum modeling. *Journal of Voice, 26*(6), 816.e21–816.e29. https://doi.org/10.1016/j.jvoice.2012.04.010

**Anderson, K. R., Oleson, J. J., & Anthony, T. R.** (2014). Variability in coefficient of restitution in human facial skin. *Skin Research and Technology, 20*(3), 355–362. https://doi.org/10.1111/srt.12126

**Behrman, A., Dahl, L. D., Abramson, A. L., & Schutte, H. K.** (2003). Anterior-posterior and medial compression of the supraglottis: Signs of nonorganic dysphonia or normal postures? *Journal of Voice, 17*(3), 403–410. https://doi.org/10.1067/S0892-1997(03)00018-3

**Birk, V., Kniesburges, S., Semmler, M., Berry, D. A., Bohr, C., Döllinger, M., & Schützenberger, A.** (2017). Influence of glottal closure on the phonatory process in ex vivo porcine larynges. *The Journal of the Acoustical Society of America, 142*(4), 2197–2207. https://doi.org/10.1121/1.5007952

**Björklund, S., & Sundberg, J.** (2016). Relationship between subglottal pressure and sound pressure level in untrained voices. *Journal of Voice, 30*(1), 15–20. https://doi.org/10.1016/j.jvoice.2015.03.006

**Catford, J. C.** (1988). *A practical introduction to phonetics*. Clarendon Press.

**Chan, R. W., Fu, M., Young, L., & Tirunagari, N.** (2007). Relative contributions of collagen and elastin to elasticity of the vocal fold under tension. *Annals of Biomedical Engineering, 35*(8), 1471–1483. https://doi.org/10.1007/s10439-007-9314-x

**Chan, R. W., & Rodriguez, M. L.** (2008). A simple-shear rheometer for linear viscoelastic characterization of vocal fold tissues at phonatory frequencies. *The Journal of the Acoustical Society of America, 124*(2), 1207–1219. https://doi.org/10.1121/1.2946715

**Chan, R. W., & Titze, I. R.** (1999). Viscoelastic shear properties of human vocal fold mucosa: Measurement methodology and empirical results. *The Journal of the Acoustical Society of America, 106*(4), 2008–2021. https://doi.org/10.1121/1.427947

**Chen, G., Kreiman, J., Shue, Y.-L., & Alwan, A.** (2011). *Acoustic correlates of glottal gaps*. INTERSPEECH 2011, 12th Annual Conference of the International Speech Communication Association, Florence, Italy.

**Chen, L., & Mongeau, L.** (2011). Verification of two minimally invasive methods for the estimation of the contact pressure in human vocal folds during phonation. *The Journal of the Acoustical Society of America, 130*(3), 1618–1627. https://doi.org/10.1121/1.3613708

**Chhetri, D. K., Zhang, Z., & Neubauer, J.** (2011). Measurement of young's modulus of vocal folds by indentation. *Journal of Voice, 25*(1), 1–7. https://doi.org/10.1016/j.jvoice.2009.09.005

**Choi, J., Son, Y. I., So, Y. K., Byun, H., Lee, E. K., & Yun, Y. S.** (2012). Posterior glottic gap and age as factors predicting voice outcome of injection laryngoplasty in patients with unilateral vocal fold paralysis. *The Journal of Laryngology and Otology, 126*(3), 260–266. https://doi.org/10.1017/S0022215111002702

**Cielo, C. A., Schwarz, K., Finger, L. S., Lima, J. M., & Christmann, M. K.** (2019). Glottal closure in women with no voice complaints or laryngeal disorders. *International Archives of Otorhinolaryngology, 23*(04), e384–e388. https://doi.org/10.1055/s-0038-1676108

**Comley, K., & Fleck, N.** (2012). The compressive response of porcine adipose tissue from low to high strain rate. *International Journal of Impact Engineering, 46,* 1–10. https://doi.org/10.1016/j.ijimpeng.2011.12.009

**Cranen, B., & Schroeter, J.** (1995). Modeling a leaky glottis. *Journal of Phonetics, 23*(1–2), 165–177. https://doi.org/10.1016/S0095-4470(95)80040-9

**DeJonckere, P. H., & Lebacq, J.** (2020). Vocal fold collision speed in vivo: The effect of loudness. *Journal of Voice*. Advance online publication. https://doi.org/10.1016/j.jvoice.2020.08.025

**Díaz-Cádiz, M. E., Peterson, S. D., Galindo, G. E., Espinoza, V. M., Motie-Shirazi, M., Erath, B. D., & Zañartu, M.** (2019). Estimating vocal fold contact pressure from raw laryngeal high-speed videoendoscopy using a Hertz contact model. *Applied Sciences, 9*(11), 2384. https://doi.org/10.3390/app9112384

**Dikkers, F. G., & Nikkels, P. G. J.** (1999). Lamina propria of the mucosa of benign lesions of the vocal folds. *The Laryngoscope, 109*(10), 1684–1689. https://doi.org/10.1097/00005537-199910000-00025

**Dion, G. R., Coelho, P. G., Teng, S., Janal, M. N., Amin, M. R., & Branski, R. C.** (2017). Dynamic nanomechanical analysis of the vocal fold structure in excised larynges. *The Laryngoscope, 127*(7), E225–E230. https://doi.org/10.1002/lary.26410

**Döllinger, M., & Berry, D. A.** (2006). Visualization and quantification of the medial surface dynamics of an excised human vocal fold during phonation. *Journal of Voice, 20*(3), 401–413. https://doi.org/10.1016/j.jvoice.2005.08.003

**Döllinger, M., Berry, D. A., & Kniesburges, S.** (2016). Dynamic vocal fold parameters with changing adduction in ex-vivo hemilarynx experiments. *The Journal of the Acoustical Society of America, 139*(5), 2372–2385. https://doi.org/10.1121/1.4947044

**Döllinger, M., Berry, D. A., Luegmair, G., Hüttner, B., & Bohr, C.** (2012). Effects of the epilarynx area on vocal fold dynamics and the primary voice signal. *Journal of Voice, 26*(3), 285–292. https://doi.org/10.1016/j.jvoice.2011.04.009

**Döllinger, M., Berry, D. A., & Montequin, D. W.** (2006). The influence of epilarynx area on vocal fold dynamics. *Otolaryngology—Head & Neck Surgery, 135*(5), 724–729. https://doi.org/10.1016/j.otohns.2006.04.007

**Edelsten, L., Jeffrey, J. E., Burgin, L. V., & Aspden, R. M.** (2010). Viscoelastic deformation of articular cartilage during impact loading. *Soft Matter, 6*(20), 5206–5212. https://doi.org/10.1039/c0sm00097c

**Erath, B. D., Zañartu, M., & Peterson, S. D.** (2017). Modeling viscous dissipation during vocal fold contact: The influence of tissue viscosity and thickness with implications for hydration. *Biomechanics and Modeling in Mechanobiology, 16*(3), 947–960. https://doi.org/10.1007/s10237-016-0863-5

**Espinoza, V. M., Mehta, D. D., Van Stan, J. H., Hillman, R. E., & Zañartu, M.** (2020). Glottal aerodynamics estimated from neck-surface vibration in women with phonotraumatic and nonphonotraumatic vocal hyperfunction. *Journal of Speech, Language, and Hearing Research, 63*(9), 2861–2869. https://doi.org/10.1044/2020_JSLHR-20-00189

**Espinoza, V. M., Zañartu, M., Van Stan, J. H., Mehta, D. D., & Hillman, R. E.** (2017). Glottal aerodynamic measures in women with phonotraumatic and nonphonotraumatic vocal hyperfunction. *Journal of Speech, Language, and Hearing Research, 60*(8), 2159–2169. https://doi.org/10.1044/2017_JSLHR-S-16-0337

**Fritzen, B., Hammarberg, B., Gauffin, J., Karlsson, I., & Sundberg, J.** (1986). Breathiness and insufficient vocal fold closure. *Journal of Phonetics, 14*(3–4), 549–553. https://doi.org/10.1016/S0095-4470(19)30705-3

**Galindo, G. E., Peterson, S. D., Erath, B. D., Castro, C., Hillman, R. E., & Zañartu, M.** (2017). Modeling the pathophysiology of phonotraumatic vocal hyperfunction with a triangular glottal model of the vocal folds. *Journal of Speech, Language, and Hearing Research, 60*(9), 2452–2471. https://doi.org/10.1044/2017_JSLHR-S-16-0412

**Gray, S. D., & Titze, I. R.** (1988). Histologic investigation of hyperphonated canine vocal cords. *Annals of Otology, Rhinology & Laryngology, 97*(4), 381–388. https://doi.org/10.1177/000348948809700410

**Gunter, H. E., Howe, R. D., Zeitels, S. M., Kobler, J. B., & Hillman, R. E.** (2005). Measurement of vocal fold collision forces during phonation: Methods and preliminary data. *Journal of Speech, Language, and Hearing Research, 48*(3), 567–576. https://doi.org/10.1044/1092-4388(2005/039)

**Hanson, H. M.** (1997). Glottal characteristics of female speakers: Acoustic correlates. *The Journal of the Acoustical Society of America, 101*(1), 466–481. https://doi.org/10.1121/1.417991

**Harrison, P.** (2013). *Making accurate formant measurements: An empirical investigation of the influence of the measurement tool, analysis settings and speaker on formant measurements*. University of York.

**Herbst, C. T., Hess, M., Müller, F., Švec, J. G., & Sundberg, J.** (2015). Glottal adduction and subglottal pressure in singing. *Journal of Voice, 29*(4), 391–402. https://doi.org/10.1016/j.jvoice.2014.08.009

**Hess, M. M., Verdolini, K., Bierhals, W., Mansmann, U., & Gross, M.** (1998). Endolaryngeal contact pressures. *Journal of Voice, 12*(1), 50–67. https://doi.org/10.1016/S0892-1997(98)80075-1

**Hillman, R. E., Holmberg, E. B., Perkell, J. S., Walsh, M., & Vaughan, C.** (1989). Objective assessment of vocal hyperfunction: An experimental framework and initial results. *Journal of Speech and Hearing Research, 32*(2), 373–392. https://doi.org/10.1044/jshr.3202.373

**Hillman, R. E., Stepp, C. E., Van Stan, J. H., Zañartu, M., & Mehta, D. D.** (2020). An updated theoretical framework for vocal hyperfunction. *American Journal of Speech-Language Pathology, 29*(4), 2254–2260. https://doi.org/10.1044/2020_AJSLP-20-00104

**Holmberg, E. B., Hillman, R. E., Hammarberg, B., Södersten, M., & Doyle, P.** (2001). Efficacy of a behaviorally based voice therapy protocol for vocal nodules. *Journal of Voice, 15*(3), 395–412. https://doi.org/10.1016/S0892-1997(01)00041-8

**Holmberg, E. B., Hillman, R. E., & Perkell, J. S.** (1988). Glottal airflow and transglottal air pressure measurements for male and female speakers in soft, normal, and loud voice. *The Journal of the Acoustical Society of America, 84*(2), 511–529. https://doi.org/10.1121/1.396829

**Horáček, J., Bula, V., Radolf, V., & Šidlof, P.** (2016). Impact stress in a self-oscillating model of human vocal folds. *Advances in Vibration Engineering, 13*.

**Isshiki, N.** (1964). Regulatory mechanism of voice intensity variation. *Journal of Speech and Hearing Research, 7*(1), 17–29. https://doi.org/10.1044/jshr.0701.17

**Jiang, J. J., & Titze, I. R.** (1994). Measurement of vocal fold intraglottal pressure and impact stress. *Journal of Voice, 8*(2), 132–144. https://doi.org/10.1016/S0892-1997(05)80305-4

**Jones, C. L., Achuthan, A., & Erath, B. D.** (2015). Modal response of a computational vocal fold model with a substrate layer of adipose tissue. *The Journal of the Acoustical Society of America, 137*(2), EL158–EL164. https://doi.org/10.1121/1.4905892

**Kania, R. E., Hans, S., Hartl, D. M., Clement, P., Crevier-Buchman, L., & Brasnu, D. F.** (2004). Variability of electroglottographic glottal closed quotients: Necessity of standardization to obtain normative values. *Archives of Otolaryngology—Head & Neck Surgery, 130*(3), 349–352. https://doi.org/10.1001/archotol.130.3.349

**Kojima, T., Van Deusen, M., Jerome, W. G., Garrett, C. G., Sivasankar, M. P., Novaleski, C. K., & Rousseau, B.** (2014). Quantification of acute vocal fold epithelial surface damage with increasing time and magnitude doses of vibration exposure. *PLOS ONE, 9*(3), Article e91615. https://doi.org/10.1371/journal.pone.0091615

**Ladefoged, P., & McKinney, N. P.** (1963). Loudness, sound pressure, and subglottal pressure in speech. *The Journal of the Acoustical Society of America, 35*(4), 454–460. https://doi.org/10.1121/1.1918503

**Levendoski, E. E., Leydon, C., & Thibeault, S. L.** (2014). Vocal fold epithelial barrier in health and injury: A research review.

*Journal of Speech, Language, and Hearing Research, 57*(5), 1679–1691. https://doi.org/10.1044/2014_JSLHR-S-13-0283

**Linville, S. E.** (1992). Glottal gap configurations in two age groups of women. *Journal of Speech and Hearing Research, 35*(6), 1209–1215. https://doi.org/10.1044/jshr.3506.1209

**Lohscheller, J., Švec, J. G., & Döllinger, M.** (2013). Vocal fold vibration amplitude, open quotient, speed quotient and their variability along glottal length: Kymographic data from normal subjects. *Logopedics Phoniatrics Vocology, 38*(4), 182–192. https://doi.org/10.3109/14015439.2012.731083

**Mehta, D. D., Kobler, J. B., Zeitels, S. M., Zañartu, M., Erath, B. D., Motie-Shirazi, M., Peterson, S. D., Petrillo, R. H., & Hillman, R. E.** (2019). Toward development of a vocal fold contact pressure probe: Bench-top validation of a dual-sensor probe using excised human larynx models. *Applied Sciences, 9*(20), 4360. https://doi.org/10.3390/app9204360

**Mehta, D. D., Kobler, J. B., Zeitels, S. M., Zañartu, M., Ibarra, E. J., Alzamendi, G. A., Manriquez, R., Erath, B. D., Peterson, S. D., Petrillo, R. H., & Hillman, R. E.** (2021). Direct measurement and modeling of intraglottal, subglottal, and vocal fold collision pressures during phonation in an individual with a hemilaryngectomy. *Applied Sciences, 11*(16), 7256. https://doi.org/10.3390/app11167256

**Mendelsohn, A. H., Sung, M. W., Berke, G. S., & Chhetri, D. K.** (2007). Strobokymographic and videostroboscopic analysis of vocal fold motion in unilateral superior laryngeal nerve paralysis. *Annals of Otology, Rhinology, & Laryngology, 116*(2), 85–91. https://doi.org/10.1177/000348940711600202

**Migimatsu, K., & Tokuda, I. T.** (2019). Experimental study on nonlinear source–filter interaction using synthetic vocal fold models. *The Journal of the Acoustical Society of America, 146*(2), 983–997. https://doi.org/10.1121/1.5120618

**Min, Y. B., Titze, I. R., & Alipour-Haghighi, F.** (1995). Stress–strain response of the human vocal ligament. *Annals of Otology, Rhinology & Laryngology, 104*(7), 563–569. https://doi.org/10.1177/000348949510400711

**Morrison, M. D., Nichol, H., & Rammage, L. A.** (1986). Diagnostic criteria in functional dysphonia. *The Laryngoscope, 96*(1), 1–8. https://doi.org/10.1288/00005537-198601000-00001

**Morrison, M. D., Rammage, L. A., Belisle, G. M., Pullan, C. B., & Nichol, H.** (1983). Muscular tension dysphonia. *The Journal of Otolaryngology, 12*(5), 302–306.

**Motie-Shirazi, M., Zañartu, M., Peterson, S. D., & Erath, B. D.** (2021a). Vocal fold dynamics in a synthetic self-oscillating model: Contact pressure and dissipated-energy dose. *The Journal of the Acoustical Society of America, 150*(1), 478–489. https://doi.org/10.1121/10.0005596

**Motie-Shirazi, M., Zañartu, M., Peterson, S. D., & Erath, B. D.** (2021b). Vocal fold dynamics in a synthetic self-oscillating model: Intraglottal aerodynamic pressure and energy. *The Journal of the Acoustical Society of America, 150*(2), 1332–1345. https://doi.org/10.1121/10.0005882

**Motie-Shirazi, M., Zañartu, M., Peterson, S. D., Mehta, D. D., Kobler, J. B., Hillman, R. E., & Erath, B. D.** (2019). Toward development of a vocal fold contact pressure probe: Sensor characterization and validation using synthetic vocal fold models. *Applied Sciences, 9*(15), 3002. https://doi.org/10.3390/app9153002

**Murray, P. R., & Thomson, S. L.** (2012). Vibratory responses of synthetic, self-oscillating vocal fold models. *The Journal of the Acoustical Society of America, 132*(5), 3428–3438. https://doi.org/10.1121/1.4754551

**Nguyen, D. D., Kenny, D. T., Tran, N. D., & Livesey, J. R.** (2009). Muscle tension dysphonia in Vietnamese female teachers. *Journal of Voice, 23*(2), 195–208. https://doi.org/10.1016/j.jvoice.2007.09.003

**Omori, K., Slavit, D. H., Kacker, A., & Blaugrund, S. M.** (1996). Quantitative videostroboscopic measurement of glottal gap and vocal function: An analysis of thyroplasty type I. *Annals of Otology, Rhinology & Laryngology, 105*(4), 280–285. https://doi.org/10.1177/000348949610500407

**Oren, L., Dembinski, D., Gutmark, E., & Khosla, S.** (2014). Characterization of the vocal fold vertical stiffness in a canine model. *Journal of Voice, 28*(3), 297–304. https://doi.org/10.1016/j.jvoice.2013.11.001

**Park, J. B., & Mongeau, L.** (2008). Experimental investigation of the influence of a posterior gap on glottal flow and sound. *The Journal of the Acoustical Society of America, 124*(2), 1171–1179. https://doi.org/10.1121/1.2945116

**Patel, R. R., Dixon, A., Richmond, A., & Donohue, K. D.** (2012). Pediatric high speed digital imaging of vocal fold vibration: A normative pilot study of glottal closure and phase closure characteristics. *International Journal of Pediatric Otorhinolaryngology, 76*(7), 954–959. https://doi.org/10.1016/j.ijporl.2012.03.004

**Perkell, J. S., Hillman, R. E., & Holmberg, E. B.** (1994). Group differences in measures of voice production and revised values of maximum airflow declination rate. *The Journal of the Acoustical Society of America, 96*(2), 695–698. https://doi.org/10.1121/1.410307

**Reidenbach, M. M.** (1996). The paraglottic space and transglottic cancer: Anatomical considerations. *Clinical Anatomy, 9*(4), 244–251. https://doi.org/10.1002/(SICI)1098-2353(1996)9:4

**Rousseau, B., Suehiro, A., Echemendia, N., & Sivasankar, M.** (2011). Raised intensity phonation compromises vocal fold epithelial barrier integrity. *The Laryngoscope, 121*(2), 346–351. https://doi.org/10.1002/lary.21364

**Scherer, R. C., Frazer, B., & Zhai, G.** (2013). Modeling flow through the posterior glottal gap. *Proceedings of Meetings on Acoustics ICA2013, 19*(1), 60240.

**Schneider, B., & Bigenzahn, W.** (2003). Influence of glottal closure configuration on vocal efficacy in young normal-speaking women. *Journal of Voice, 17*(4), 468–480. https://doi.org/10.1067/S0892-1997(03)00065-1

**Spencer, M., Siegmund, T., & Mongeau, L.** (2008). Determination of superior surface strains and stresses, and vocal fold contact pressure in a synthetic larynx model using digital image correlation. *The Journal of the Acoustical Society of America, 123*(2), 1089–1103. https://doi.org/10.1121/1.2821412

**Stager, S. V., Bielamowicz, S. A., Regnell, J. R., Gupta, A., & Barkmeier, J. M.** (2000). Supraglottic activity: Evidence of vocal hyperfunction or laryngeal articulation? *Journal of Speech, Language, and Hearing Research, 43*(1), 229–238. https://doi.org/10.1044/jslhr.4301.229

**Story, B. H.** (2008). Comparison of magnetic resonance imaging-based vocal tract area functions obtained from the same speaker in 1994 and 2002. *The Journal of the Acoustical Society of America, 123*(1), 327–335. https://doi.org/10.1121/1.2805683

**Story, B. H., & Titze, I. R.** (1995). Voice simulation with a body-cover model of the vocal folds. *The Journal of the Acoustical Society of America, 97*(2), 1249–1260. https://doi.org/10.1121/1.412234

**Story, B. H., Titze, I. R., & Hoffman, E. A.** (1996). Vocal tract area functions from magnetic resonance imaging. *The Journal of the Acoustical Society of America, 100*(1), 537–554. https://doi.org/10.1121/1.415960

**Sundberg, J.** (1988). Vocal tract resonance in singing. *The NATS Journal, 44*(4), 11–20.

**Syndergaard, K. L., Dushku, S., & Thomson, S. L.** (2017). Electrically conductive synthetic vocal fold replicas for voice

production research. *The Journal of the Acoustical Society of America, 142*(1), EL63–EL68. https://doi.org/10.1121/1.4990540

**Thomson, S. L., Mongeau, L., & Frankel, S. H.** (2005). Aerodynamic transfer of energy to the vocal folds. *The Journal of the Acoustical Society of America, 118*(3), 1689–1700. https://doi.org/10.1121/1.2000787

**Titze, I. R.** (2006). Voice training and therapy with a semi-occluded vocal tract: Rationale and scientific underpinnings. *Journal of Speech, Language, and Hearing Research, 49*(2), 448–459. https://doi.org/10.1044/1092-4388(2006/035)

**Titze, I. R., & Alipour, F.** (2006). *The myoelastic aerodynamic theory of phonation*. National Center for Voice and Speech.

**Titze, I. R., & Hunter, E. J.** (2015). Comparison of vocal vibration-dose measures for potential-damage risk criteria. *Journal of Speech, Language, and Hearing Research, 58*(5), 1425–1439. https://doi.org/10.1044/2015_JSLHR-S-13-0128

**Titze, I. R., Riede, T., & Popolo, P.** (2008). Nonlinear source–filter coupling in phonation: Vocal exercises. *The Journal of the Acoustical Society of America, 123*(4), 1902–1915. https://doi.org/10.1121/1.2832339

**Titze, I. R., & Story, B. H.** (1997). Acoustic interactions of the voice source with the lower vocal tract. *The Journal of the Acoustical Society of America, 101*(4), 2234–2243. https://doi.org/10.1121/1.418246

**Titze, I. R., & Sundberg, J.** (1998). Vocal intensity in speakers and singers. *The Journal of the Acoustical Society of America, 91*(5), 2936–2946. https://doi.org/10.1121/1.402929

**Titze, I. R., Svec, J. G., & Popolo, P. S.** (2003). Vocal dose measures: Quantifying accumulated vibration exposure in vocal fold tissues. *Journal of Speech, Language, and Hearing Research, 46*(4), 919–932. https://doi.org/10.1044/1092-4388(2003/072)

**Verdolini, K., Hess, M. M., Titze, I. R., Bierhals, W., & Gross, M.** (1999). Investigation of vocal fold impact stress in human subjects. *Journal of Voice, 13*(2), 184–202. https://doi.org/10.1016/S0892-1997(99)80022-8

**Weiss, S., Sutor, A., Rupitsch, S. J., Kniesburges, S., Döllinger, M., & Lerch, R.** (2013). Development of a small film sensor for the estimation of the contact pressure of artificial vocal folds. *Proceedings of Meetings on Acoustics ICA2013, 19*(1), 60307.

**Wu, L., & Zhang, Z.** (2021). Impact of the paraglottic space on voice production in an MRI-based vocal fold model. *Journal of Voice*. Advance online publication. https://doi.org/10.1016/J.JVOICE.2021.02.021

**Yanagisawa, E., Estill, J., Kmucha, S. T., & Leder, S. B.** (1989). The contribution of aryepiglottic constriction to "ringing" voice quality—A videolaryngoscopic study with acoustic analysis. *Journal of Voice, 3*(4), 342–350. https://doi.org/10.1016/S0892-1997(89)80057-8

**Zañartu, M., Galindo, G. E., Erath, B. D., Peterson, S. D., Wodicka, G. R., & Hillman, R. E.** (2014). Modeling the effects of a posterior glottal opening on vocal fold dynamics with implications for vocal hyperfunction. *The Journal of the Acoustical Society of America, 136*(6), 3262–3271. https://doi.org/10.1121/1.4901714

**Zhang, Z.** (2015). Regulation of glottal closure and airflow in a three-dimensional phonation model: Implications for vocal intensity control. *The Journal of the Acoustical Society of America, 137*(2), 898–910. https://doi.org/10.1121/1.4906272

**Zhang, Z.** (2016). Cause–effect relationship between vocal fold physiology and voice production in a three-dimensional phonation model. *The Journal of the Acoustical Society of America, 139*(4), 1493–1507. https://doi.org/10.1121/1.4944754

**Zhang, Z.** (2019). Compensation strategies in voice production with glottal insufficiency. *Journal of Voice, 33*(1), 96–102. https://doi.org/10.1016/j.jvoice.2017.10.002

**Zhang, Z.** (2021). Interaction between epilaryngeal and laryngeal adjustments in regulating vocal fold contact pressure. *JASA Express Letters, 1*(2), 025201. https://doi.org/10.1121/10.0003393

**Zhang, Z., & Hieu Luu, T.** (2012). Asymmetric vibration in a two-layer vocal fold model with left-right stiffness asymmetry: Experiment and simulation. *The Journal of the Acoustical Society of America, 132*(3), 1626–1635. https://doi.org/10.1121/1.4739437

**Zhang, Z., Kreiman, J., Gerratt, B. R., & Garellek, M.** (2013). Acoustic and perceptual effects of changes in body layer stiffness in symmetric and asymmetric vocal fold models. *The Journal of the Acoustical Society of America, 133*(1), 453–462. https://doi.org/10.1121/1.4770235

**Zhang, Z., Neubauer, J., & Berry, D. A.** (2006). The influence of subglottal acoustics on laboratory models of phonation. *The Journal of the Acoustical Society of America, 120*(3), 1558–1569. https://doi.org/10.1121/1.2225682

**Zhao, R., Cai, Y., & Wang, H.** (1991). Pathological changes of hyperphonated cat vocal folds. *Auris Nasus Larynx, 18*(1), 55–59. https://doi.org/10.1016/S0385-8146(12)80250-1